Hindawi Publishing Corporation
Journal of Nanomaterials
Volume 2015, Article ID 151532, 6 pages
http://dx.doi.org/10.1155/2015/151532

Research Article

Synthesis of High Crystalline Al-Doped ZnO Nanopowders from Al_2O_3 and ZnO by Radio-Frequency Thermal Plasma

Min-Kyeong Song,[1] Mi-Yeon Lee,[1,2] Jun-Ho Seo,[1,2] Min-Ho Kim,[2] and Shi-Young Yang[3]

[1]*Department of Plasma Application Engineering, Chonbuk National University, Jeonbuk 561-756, Republic of Korea*
[2]*High Enthalpy Plasma Research Center, Chonbuk National University, Jeonbuk 561-756, Republic of Korea*
[3]*Graduate School of Flexible & Printable Electronics, Chonbuk National University, Jeonbuk 561-756, Republic of Korea*

Correspondence should be addressed to Min-Ho Kim; minho@jbnu.ac.kr and Shi-Young Yang; yangsy@jbnu.ac.kr

Received 15 May 2015; Accepted 30 July 2015

Academic Editor: Kyong-Yop Rhee

High crystalline Al-doped ZnO (AZO) nanopowders were prepared by in-flight treatment of ZnO and Al_2O_3 in Radio-Frequency (RF) thermal plasma. Micron-sized (~1 μm) ZnO and Al_2O_3 powders were mixed at Al/Zn ratios of 3.3 and 6.7 at.% and then injected into the RF thermal plasma torch along the centerline at a feeding rate of 6.6 g/min. The RF thermal plasma torch system was operated at the plate power level of ~140 kVA to evaporate the mixture oxides and the resultant vapor species were condensed into solid particles by the high flow rate of quenching gas (~7000 slpm). The FE-SEM images of the as-treated powders showed that the multipod shaped and the whisker type nanoparticles were mainly synthesized. In addition, these nanocrystalline structures were confirmed as the single phase AZO nanopowders with the hexagonal wurtzite ZnO structure by the XRD patterns and FE-TEM results with the SAED image. However, the composition changes of 0.3 and 1.0 at.% were checked for the as-synthesized AZO nanopowders at Al/Zn ratios of 3.3 and 6.7 at.%, respectively, by the XRF data, which can require the adjustment of Al/Zn in the mixture precursors for the applications of high Al doping concentrations.

1. Introduction

Zinc oxide is a typical n-type semiconductor with transparency to visible light [1–3]. Because of these electrical and optical properties, ZnO nanopowders have attracted much attention as the building block for transparent electrodes in RFID tags, light emitting diodes (LEDs), and solar cells [4–6]. Furthermore, as an earth-abundant material, ZnO can be used as an alternative to indium tin oxide (ITO), whose supply may be depleted in the near future. Compared with the electrical conductivity of indium tin oxide (ITO), however, that of ZnO needs to be improved for practical application as a TCO (transparent conductive oxide) material. For this purpose, ZnO is often doped with group III and IV metals, such as Al, Ga, and In [2, 7–9]. By acting as an impurity in the ZnO structure, these metals can enhance the high n-type conductivity of the doped ZnO as well as the optical transparency [7–9]. Accordingly, many efforts have been made to offer the doped ZnO nanopowders as the building block for TCO electrodes. Among them, the Al-doped ZnO (AZO) nanostructures are promising as a low-cost TCO material to substitute the ITOs because Al metal is a typical earth-abundant material. In addition, Al metal can greatly improve the electrical conductivity of ZnO [10]. For example, AZO nanowires have been reported to show a steep increase of the electrical conductivity up to 9.73×10^{-5} S/cm compared with the value of 2.55×10^{-5} S/cm for the electrical conductivity of the pure ZnO nanowires [10]. The physical properties and the morphology of AZO nanopowders strongly depend on their preparation methods [7, 11, 12]. Conventional wet chemical processes including precipitation, sol-gel, and hydrothermal routes can produce AZO nanopowders with the specific compositions and various morphologies from flower-like ones to nanowhisker types [7, 11, 12]. However, these conventional processes may produce nanopowders of poor crystalline quality because of the relatively low synthesis temperatures, in which case an additional calcination process would be needed to produce nanopowders of high crystalline quality.

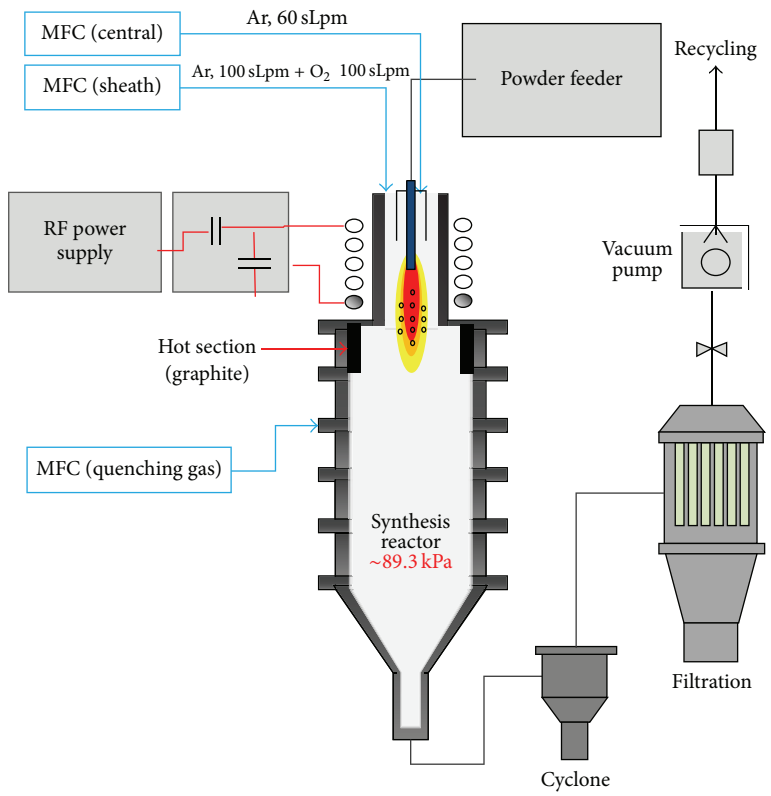

Figure 1: A schematic of the RF thermal plasma system for the synthesis of nanosized AZO powders.

Recently, RF (Radio-Frequency) thermal plasma has been gradually adopted as a unique heat source in making nanosized powders [13–17]. Since no electrode is required for sustaining plasma state, RF plasma torches can produce high enthalpy flow fields without electrode erosion and arc jet fluctuation, which are inevitable in the applications based on DC (Direct Current) arc plasma torches. These well-known advantages of RF plasma torch can be beneficial to the synthesis of nanocomposite powders by the in-flight heat treatment of mixture precursors. As for the doped ZnO, for example, Cheng et al. reported that AZO nanopowders can be prepared by RF thermal plasma treatment of the aqueous suspension with an oxide mixture of 10 wt.% [17]. Although Cheng et al.'s work was also intended to utilize those advantages of RF plasma torch for the synthesis of AZO nanopowders, the in-flight treated aqueous solution may bring the poor crystallinity to the as-prepared nanopowders due to the latent heat of water vaporization and relatively low RF power level (~21 kW) [17, 18]. Considering the crystallinity of the as-prepared powders and the simplification of the preparation process, we employed a solid mixture consisting of Al_2O_3 and ZnO powders as a precursor for RF thermal plasma synthesis of AZO nanopowders in this work. By removing the vaporization process of water and using a high-powered (~140 kVA) RF thermal plasma system, the plasma enthalpy can be used efficiently in heating not only the injected oxide powders but also the as-synthesized particles.

2. Experimental Details

2.1. RF Thermal Plasma Synthesis of Al-Doped ZnO Nanopowders. A schematic of the commercial RF thermal plasma system used in this work is illustrated in Figure 1. In this system, electromagnetic energy with oscillation frequencies of 1–4 MHz was generated from a self-excited type RF oscillator with the maximum plate power level of 350 kW and transferred to the RF thermal plasma in an inductively coupled way through the induction coil of the RF plasma torch (Tekna, PS-100). For the confinement of the generated RF thermal plasma, a water-cooled Si_3N_4 tube with an inner diameter of 100 mm was employed inside the RF plasma torch (Tekna, PS-100), which was mounted on a 700 mm diameter × 1000 mm long synthesis reactor. The upper part of synthesis reactor was equipped with a carbon liner for thermal insulation, as shown in Figure 1. This carbon liner helped to expand the high enthalpy plasma flame in the synthesis reactor and to heat the injected oxides up to their evaporation points. Then, nanopowders were synthesized by quenching the vapor species of the injected materials. In this quenching process, a gas mixture of Ar and O_2 was poured into the synthesis reactor at a flow rate of ~7000 slpm. Finally, the synthesized nanopowders were collected at the sintered stainless-steel filters with a total surface area of 2.9 m^2.

For the preparation of the solid precursors, micron-sized powders of ZnO (~1 μm) and Al_2O_3 (~1 μm) were weighed

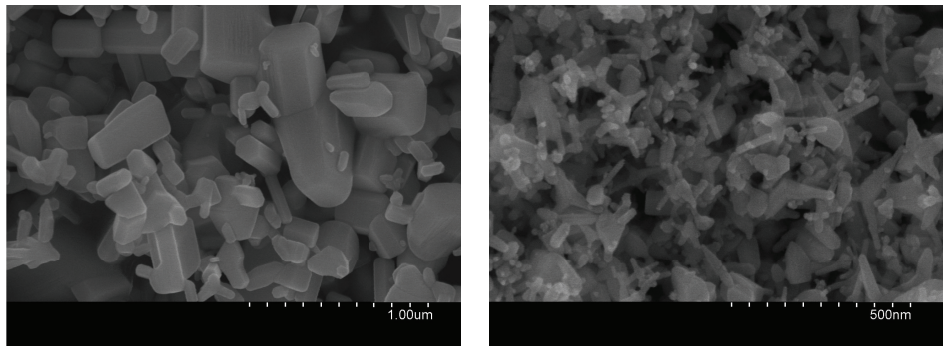

(a) (b)

Figure 2: FE-SEM images of (a) the as-mixed precursor powders and (b) the as-synthesized powders, at Al/Zn doping concentration = 3.3 at.%.

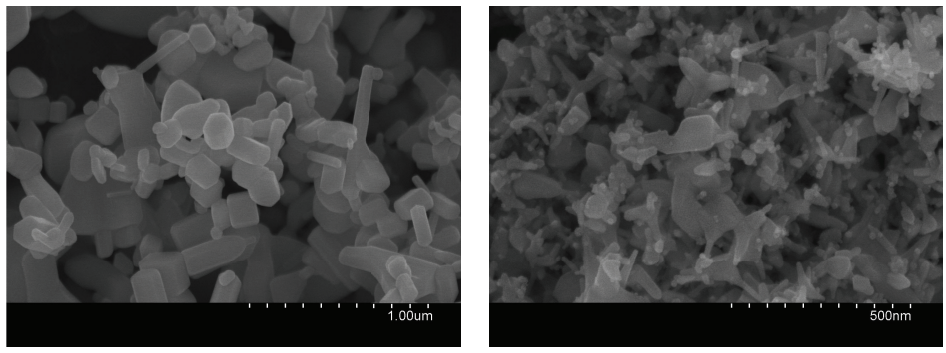

(a) (b)

Figure 3: FE-SEM images of (a) the as-mixed precursor powders and (b) the as-synthesized powders, at Al/Zn doping concentration = 6.7 at.%.

and mixed at Al/Zn ratios of 3.3 and 6.7 at.%. The mixture precursors were fed along the centerline of the RF thermal plasma torch through a water cooled injector, which was connected to the powder feeder, as shown in Figure 1. The injected precursors were treated by the RF thermal plasma generated at the plate power level of ~140 kVA and the plasma forming gas flow rate of 260 slpm, where the plasma forming gas consisted of a central gas (Ar only, 60 slpm) and a sheath gas (Ar 100 slpm and O_2 100 slpm), as depicted in Figure 1. In the RF thermal plasma system, all gases including quenching gas were designed to move continuously at the reactor pressure of 89.3 kPa by mechanical vacuum pump and gas recycling system.

2.2. Characterization of Al-Doped ZnO Nanopowders. Field emission-scanning electron microscopy (FE-SEM, S4800, Hitachi Ltd., Japan) and field emission-transmission electron microscopy (FE-TEM, JEM-2200FS, Jeol, Japan) were used to observe the particle sizes and morphologies of the mixture precursors and the RF plasma treated powders. The electron microscopes were operated at acceleration voltages of 10 kV and 200 kV, respectively. The transmission electron microscopy/energy dispersive X-ray spectroscopy (TEM-EDX, INCA X-sight, Oxford, UK) was used to observe the result of Al doping. For the preparation of TEM sample, the as-synthesized powders were dispersed in ethanol by an ultrasonic vibrator for 5 min and then loaded on a copper grid. The phase and structural analyses were carried out by X-ray diffraction (XRD, D8 Advance, Bruker, Germany) with Cu Kα radiation ($\lambda = 1.5405$ Å) at 2-theta angles ranging from 20° to 80° and scan speed of 10 min^{-1}. Finally, difference in the composition between precursors and the as-synthesized powders was checked by X-ray fluorescence analysis (XRF, S4 Pioneer, Bruker, Germany).

3. Results and Discussion

Figures 2(a) and 2(b) show the FE-SEM images of the mixture precursors and the RF plasma treated powders for Al/Zn doping concentration = 3.3 at.%, respectively. From these images, one can see that the irregular mixture precursors were mainly reformed into multipod shaped or whisker type nanocrystals after plasma processing. Figures 3(a) and 3(b) show the FE-SEM images of a similar change in the morphology and particle sizes of the mixture precursors after processing for Al/Zn doping concentration = 6.7 at.%. Since the micron-sized (~1 μm) solid precursors will be evaporated due to the huge enthalpy of the high-powered RF thermal plasma

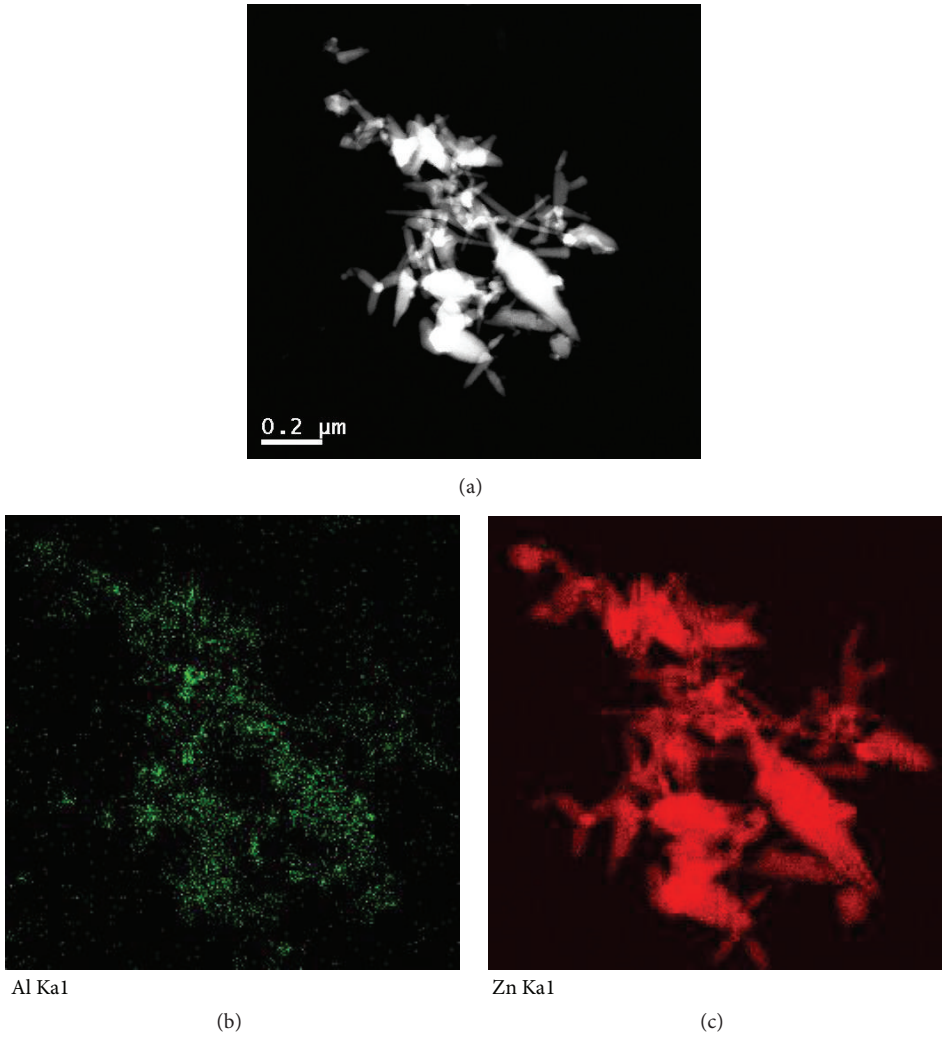

(a)

(b)

(c)

Figure 4: TEM-EDX mapping images of the as-synthesized nanopowders with multipods and whisker-like morphologies, at Al/Zn doping concentration = 6.7 at.%.

(~140 kVA), these changes in the morphology and sizes can take a place during the condensation and nucleation process of the vapor species. In these processes, accordingly, Al atoms can be expected to be doped into ZnO nanocrystals with the whisker-like morphology or the multipods. In order to confirm Al doping in the as-synthesized nanocrystals, TEM-EDX mapping images were obtained for the as-synthesized powders at Al/Zn ratio = 6.7 at.%, which are presented in Figure 4. As expected, this figure shows that the elements Al and Zn were relatively uniformly dispersed in the as-synthesized nanocrystals consisting of the multipods and the whiskers. Additionally, the SAED (Selected Area Electron Diffraction) patterns of the TEM images for the multipod and the whisker, as shown in Figures 5(a) and 5(b), reveal that the as-synthesized nanocrystals had a wurtzite structure of ZnO. Since Al elements were detected in the as-prepared powders by TEM-EDX (see Figure 4), these SAED results indicate that AZO nanopowders can be synthesized as a single phase of ZnO. The formation of the AZO nanocrystals with a single phase of ZnO can also be confirmed by comparing the XRD patterns of the mixture precursors and the as-synthesized powders, as shown in Figures 6 and 7. In Figure 6, the crystalline peaks for Al_2O_3 were not detected in the XRD graph of the as-synthesized powders, although they were present in the mixture precursors. In addition, the diffraction peaks corresponding to the wurtzite structure of ZnO shifted to higher Bragg angles (2-theta) for the as-synthesized powders as observed in Figure 7, indicating the replacement of Zn^{2+} by Al^{3+} in the ZnO lattice. Together with the TEM-EDX mapping images (see Figure 4) and SAED data (see Figures 5(a) and 5(b)) of the nanocrystals, these XRD results show that high crystalline AZO nanopowders with a single phase of ZnO were synthesized by RF thermal plasma treatment of Al_2O_3 and ZnO powders.

Finally, the change in the composition between the mixture precursors and the nanopowders was checked by XRF analyses, as listed in Table 1. In this table, one can see that the Al contents of the as-synthesized powders were reduced with the decrement of 0.3 and 1.0 at.% for the Al/Zn ratio = 3.3 at.% and 6.7 at.%, respectively. These changes of Al content

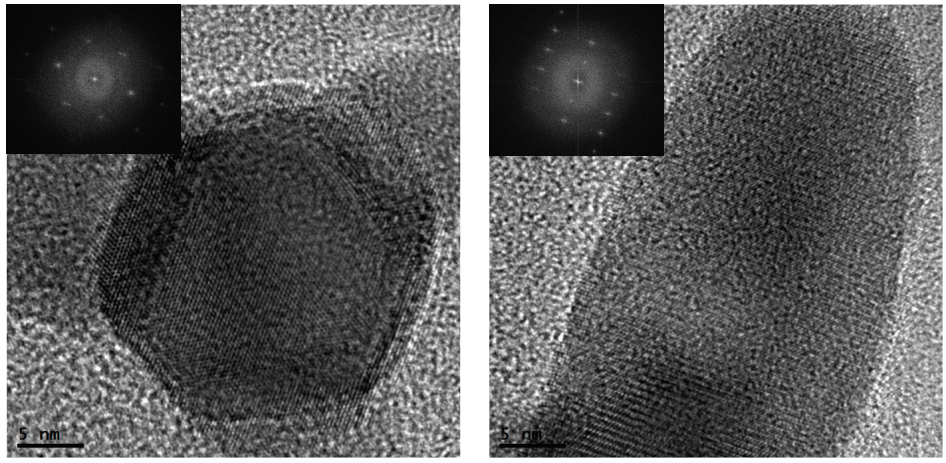

(a) (b)

Figure 5: HR-TEM images of the as-synthesized nanocrystals with morphologies of (a) a multipod and (b) a whisker, at Al/Zn doping concentration = 6.7 at.%. The insets represent the selected area diffraction patterns corresponding to each particle in HR-TEM images.

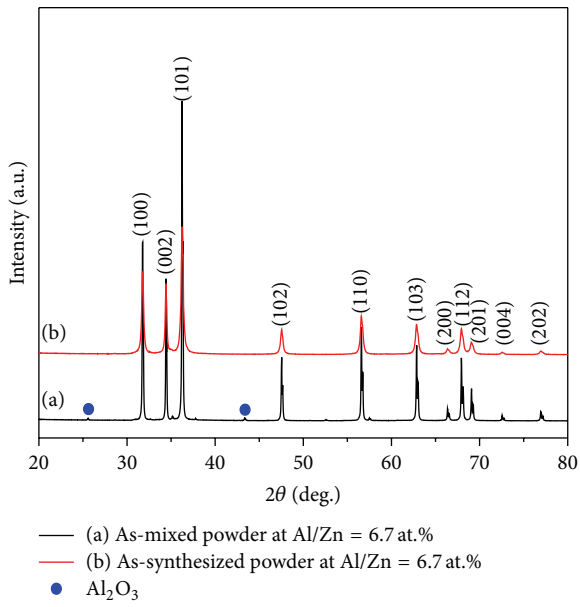

Figure 6: XRD patterns of (a) the as-mixed precursor powders and (b) the as-synthesized powders, at Al/Zn doping concentrations = 6.7 at.%.

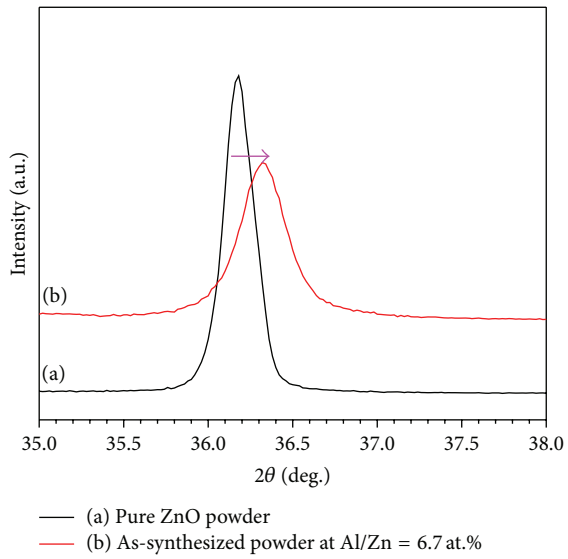

Figure 7: Comparison of XRD patterns between the pure ZnO powders and the as-synthesized powders. The main peak corresponding to ZnO wurtzite structure shifted to the higher Bragg angle (2-theta) due to the incorporation of the Al cation into the ZnO lattice.

may be attributed to not only the relatively complicated vapor species generated from Al_2O_3 at high temperatures but also their cocondensation processes for the synthesis of AZO nanopowders. For example, ZnO is simply decomposed into Zn and O at its decomposition point of 2,248 K [19]. During the quenching process, accordingly, Zn element has a single route to the formation of AZO nanocomposite. Since Al_2O_3 can be vaporized into Al and aluminium suboxides such as AlO, Al_2O, and AlO_2, around the boiling point of Al_2O_3 (~3,000 K) [19, 20], however, Al elements participating in the synthesis of AZO nanocomposite come from not only Al but also various aluminium suboxides such as AlO, Al_2O, and AlO_2, which can exist in the gas phase at different temperature ranges. As a result, some of the suboxides can be oxidized into Al_2O_3 without participating in the cocondensation of ZnO vapor species, which may lead to the Zn rich AZO nanoparticles collected at filtration as listed in Table 1 although the exact mechanism has not been clarified.

4. Conclusion

In summary, high crystalline Al-doped ZnO nanopowders were synthesized by RF thermal plasma treatment of Al_2O_3 and ZnO solid mixture precursors. From the FE-SEM images

Table 1: Relative cation composition changes between the as-mixed precursors and the as-synthesized powders based on X-ray fluorescence data.

Designed	Constituent (at.%)	Zn	Al
3.3 at.% Al-doped ZnO	Mixed precursors	96.8	3.2
	As-synthesized	97.1	2.9
	Increment	+0.3	−0.3
6.7 at.% Al-doped ZnO	Mixed precursors	93.8	6.2
	As-synthesized	94.8	5.2
	Increment	+1.0	−1.0

of the as-synthesized powders, the mixture oxide precursors were mainly reformed into nanocrystals with a multipod or a whisker morphology, which is attributed to the high crystallinity of the as-synthesized powders, as shown in XRD data. In addition, the TEM-EDX images, SAED data, and the XRD pattern of the as-synthesized powders confirmed that Al^{3+} was incorporated into the ZnO lattices of wurtzite structure, and consequently the as-synthesized AZO nanopowders had a single phase of ZnO. However, the XRF data showed a small reduction of Al content in the composition of the as-synthesized AZO nanopowder. For the practical applications requiring a high doping concentration of Al, accordingly, the experimental results indicate that the ratio of Al/Zn in the mixture precursors needs to be set higher than the targeted Al content for the adjustment of the composition of the as-synthesized AZO powder.

Conflict of Interests

The authors declare that there is no conflict of interests regarding the publication of this paper.

Acknowledgments

This research was supported by High Enthalpy Plasma Research Center funded by the Ministry of Science, ICT and Future Planning, Republic of Korea. This research was also financially supported by Components and Materials Technology Development Program (no. 10047778) and Technology Innovation Program (no. 10048910) funded by the Ministry of Trade, Industry and Energy (MI, Republic of Korea).

References

[1] A. B. Djurišić and Y. H. Leung, "Optical properties of ZnO nanostructures," *Small*, vol. 2, no. 8-9, pp. 944–961, 2006.

[2] A. Janotti and C. G. van de Walle, "Fundamentals of zinc oxide as a semiconductor," *Reports on Progress in Physics*, vol. 72, no. 12, Article ID 126501, 2009.

[3] J.-H. Lee, K.-H. Ko, and B.-O. Park, "Electrical and optical properties of ZnO transparent conducting films by the sol-gel method," *Journal of Crystal Growth*, vol. 247, no. 1-2, pp. 119–125, 2003.

[4] V. Subramanian, J. M. J. Fréchet, P. C. Chang et al., "Progress toward development of all-printed RFID tags: materials, processes, and devices," *Proceedings of the IEEE*, vol. 93, no. 7, pp. 1330–1338, 2005.

[5] H. Liu, V. Avrutin, N. Izyumskaya, Ü. Özgr, and H. Morkoç, "Transparent conducting oxides for electrode applications in light emitting and absorbing devices," *Superlattices and Microstructures*, vol. 48, no. 5, pp. 458–484, 2010.

[6] S. Rani, P. Suri, P. K. Shishodia, and R. M. Mehra, "Synthesis of nanocrystalline ZnO powder via sol-gel route for dye-sensitized solar cells," *Solar Energy Materials and Solar Cells*, vol. 92, no. 12, pp. 1639–1645, 2008.

[7] K. J. Chen, T. H. Fang, F. Y. Hung et al., "The crystallization and physical properties of Al-doped ZnO nanoparticles," *Applied Surface Science*, vol. 254, no. 18, pp. 5791–5795, 2008.

[8] X. Zhang, X. Pu, Y. Chen, X. Gu, D. Xu, and S. Zhang, "Characterization of high concentration Ga-doped ZnO nanopowders prepared by sol-gel combustion," *Materials Letters*, vol. 112, pp. 129–132, 2013.

[9] J. Jie, G. Wang, X. Han et al., "Indium-doped zinc oxide nanobelts," *Chemical Physics Letters*, vol. 387, no. 4–6, pp. 466–470, 2004.

[10] D. Lin, H. Wu, and W. Pan, "Photoswitches and memories assembled by electrospinning aluminum-doped zinc oxide single nanowires," *Advanced Materials*, vol. 19, no. 22, pp. 3968–3972, 2007.

[11] S. Suwanboon, P. Amornpitoksuk, A. Haidoux, and J. C. Tedenac, "Structural and optical properties of undoped and aluminium doped zinc oxide nanoparticles via precipitation method at low temperature," *Journal of Alloys and Compounds*, vol. 462, no. 1-2, pp. 335–339, 2008.

[12] S. Baruah and J. Dutta, "Hydrothermal growth of ZnO nanostructures," *Science and Technology of Advanced Materials*, vol. 10, no. 1, Article ID 013001, 2009.

[13] J.-H. Seo and B.-G. Hong, "Thermal plasma synthesis of nano-sized powders," *Nuclear Engineering and Technology*, vol. 44, no. 1, pp. 9–20, 2012.

[14] S.-M. Oh and T. Ishigaki, "Preparation of pure rutile and anatase TiO_2 nanopowders using RF thermal plasma," *Thin Solid Films*, vol. 457, no. 1, pp. 186–191, 2004.

[15] M.-Y. Lee, J.-S. Kim, and J.-H. Seo, "Radio-frequency thermal plasma synthesis of nano-sized indium zinc tin oxide powders with reduced indium content," *Thin Solid Films*, vol. 521, pp. 60–64, 2012.

[16] Y. Cheng, M. Shigeta, S. Choi, and T. Watanabe, "Formation mechanism of titanium boride nanoparticles by RF induction thermal plasma," *Chemical Engineering Journal*, vol. 183, pp. 483–491, 2012.

[17] H. Cheng, X. J. Xu, H. H. Hng, and J. Ma, "Characterization of Al-doped ZnO thermoelectric materials prepared by RF plasma powder processing and hot press sintering," *Ceramics International*, vol. 35, no. 8, pp. 3067–3072, 2009.

[18] L. Qian, J. Lin, and H. Xiong, "Numerical modeling in radio frequency suspension plasma spray of zirconia powders," *Plasma Chemistry and Plasma Processing*, vol. 30, no. 6, pp. 733–760, 2010.

[19] M. W. Chase Jr., *NIST-JANAF Themochemical Tables*, Monograph 9, American Institute of Physics, College Park, Md, USA, 4th edition, 1998.

[20] T. Kitamura, K. Shibata, and K. Takeda, "In-flight reduction of Fe_2O_3, Cr_2O_3, TiO_2 and Al_2O_3 by Ar-H_2 and Ar-CH_4 plasma," *ISIJ International*, vol. 33, no. 11, pp. 1150–1158, 1993.